Spring 4-14-2017

Characterization of a Small Electro-Mechanical Contact Using Non-Conventional Measurement Techniques

Kelsey M. Johnson
University of New Mexico

Kelsey M. Johnson
Candidate

Department of Mechanical Engineering, Graduate Studies
Department

This thesis is approved, and it is acceptable in quality and form for publication:

Approved by the Thesis Committee:

Dr. John J. Russell, Chairperson

Dr. Yu-Lin Shen

Dr. Jill C. Blecke

CHARACTERIZATION OF A SMALL ELECTRO-MECHANICAL CONTACT USING NON-CONVENTIONAL MEASUREMENT TECHNIQUES

by

KELSEY M. JOHNSON

B.S. MECHANICAL ENGINEERING, UNIVERSITY OF NEW MEXICO, 2015

THESIS

Submitted in Partial Fulfillment of the Requirements for the Degree of

Master of Science
Mechanical Engineering

The University of New Mexico
Albuquerque, New Mexico

May, 2017

ACKNOWLEDGEMENTS

I would like to acknowledge Dr. John J. Russell, my advisor and committee chair, for taking me on as a research student and putting up with me as I completed my research. He has always been supportive of my work and my aspirations throughout my undergraduate and graduate studies, always pushing me to go for the best.

I would also like to thank my committee members, Dr. Yu-Lin Shen and Dr. Jill C. Blecke for helping me along with my work as well, with a special thanks to Dr. Blecke. Her advice, technically and professionally, has been invaluable and I look forward to continually working with her throughout my career.

A special thanks to Sandia National Laboratories and to my managers and mentors there for providing the funding for this research. I am happy and very fortunate to be continuing my career there and pursuing research that can extend Sandia's capabilities to better serve the nation.

Thanks to Scott Smith and Dan Rohe for helping obtain some data with me.

And lastly, thanks to all my friends and family, for supporting me and putting up with me during my education and research. Your encouragement and patience is very appreciated.

CHARACTERIZATION OF A SMALL ELECTRO-MECHANICAL CONTACT USING NON-CONVENTIONAL MEASUREMENT TECHNIQUES

by

Name:
KELSEY M. JOHNSON
List of Previous Degrees:

B.S. MECHANICAL ENGINEERING, UNIVERSITY OF NEW MEXICO, 2015
M.S. MECHANICAL ENGINEERING, UNIVERSITY OF NEW MEXICO, 2017

ABSTRACT

Currently there are limitations in computing chatter behavior of small electrical contacts embedded in components using finite element models. Reduced order models (ROM) have been developed of such electrical contact sub-assemblies to assess the chatter behavior of the contacts during vibration and shock environments. The current ROM method requires experimental validation. This ROM also neglects the damping effects of the viscous fluid that typically surrounds such sub-assemblies. Dynamic ring-down testing of the electrical contacts in air was performed and will provide a validation data set for the current ROM. Additionally, dynamic ring-down testing of the electrical contact was performed in fluids of varying viscosities that will help characterize the effect of the fluid on the contact for an improved ROM.

TABLE OF CONTENTS

Chapter One: Introduction **1**
Objective and Overview 1
Background 2
Chapter Two: Experimental Setup **12**
Chapter Three: Results **19**
Data and Processing 19
Model Comparison 30
Chapter Four: Conclusion **32**
Appendix **34**
References **35**

LIST OF FIGURES

FIGURE 1: DIAGRAM OF SMALL ASSEMBLY WITH THE RECEPTACLE AS THE TEST ARTICLE (LEFT) 1
FIGURE 2: IN-PHASE AND OUT-OF-PHASE FIRST BENDING MODE SHAPES OF A TUNING FORK..... 11
FIGURE 3: TEST SETUP WITH OIL 12
FIGURE 4: TECHNICAL DRAWING FOR THE PICMA STACK ACTUATOR [14]..... 13
FIGURE 5: ACTUATOR SIGNAL 14
FIGURE 6: HOW LDV TAKES MEASUREMENTS 15
FIGURE 7: PSV-400 LDV 15
FIGURE 8: HIGH VOLTAGE AMPLIFIER 16
FIGURE 9: FREQUENCY CONTENT IN AIR (FFT) 20
FIGURE 10: FREQUENCY CONTENT IN 10CST OIL (FFT) 20
FIGURE 11: FREQUENCY CONTENT IN 20CST OIL (FFT) 20
FIGURE 12: FIRST BENDING MODE FROM 1D LDV FIGURE 13: SECOND BENDING MODE FROM 1D LDV 20
FIGURE 14: EXAMPLE OF STFT GUI WINDOW 22
FIGURE 15: FFT - FIRST BENDING MODES IN AIR 23
FIGURE 16: STFT OF FIRST OUT-OF-PHASE AND IN-PHASE BENDING MODES IN AIR 23
FIGURE 17: FFT - FIRST BENDING MODES IN 10CST OIL 24
FIGURE 18: STFT OF FIRST OUT-OF-PHASE AND IN-PHASE BENDING MODES IN 10CST OIL 24
FIGURE 19: FFT - FIRST BENDING MODES IN 20CST OIL 25
FIGURE 20: STFT OF FIRST OUT-OF-PHASE AND IN-PHASE BENDING MODES IN 20CST OIL 25
FIGURE 21: SMAC EXTRACTION - FIRST BENDING MODE, IN-PHASE 28
FIGURE 22: SMAC EXTRACTION - FIRST BENDING MODE, OUT-OF-PHASE 28
FIGURE 23: FFT FROM 3D LDV MEASUREMENT IN AIR 29
FIGURE 24: FFT - FIRST BENDING MODES IN AIR FROM 3D LDV 29
FIGURE 25: OUT-OF-PHASE FIRST BENDING MODE (LEFT) AND IN-PHASE FIRST BENDING MODE (RIGHT) FROM 3D LDV 30

LIST OF TABLES

TABLE 1: SPECIFICATIONS FOR THE PICMA STACK ACTUATORS [14] 13
TABLE 2: INSTANTANEOUS FREQUENCY AND DAMPING FOR FIRST BENDING MODES 26
TABLE 3: FIRST BENDING MODE FREQUENCY COMPARISON BETWEEN MODEL AND DATA 31

Chapter One: Introduction

Objective and Overview

This report provides a model validation data set for the reduced order model (ROM) created by Lacayo and Brake [1] that attempts to predict the chatter behavior of a small sub-assembly. A depiction of this assembly is found in Figure 1. This small system becomes active over a series of vibrations and shocks, which allows for a bifurcated electrical receptacle to make contact with a pin, resulting in a closed circuit for the rest of the larger system. Once the system is active, it remains in a vibration and shock environment and it is during this time that chatter in the system could occur. The chatter is undesirable because it increases the resistance between the electrical contact and the pin, resulting in an electrical discontinuity. The ROM being investigated lacks experimental validation while also neglecting the effects of the fluid in the system. While the model is believed to be a conservative representation of the system, this study will attempt to provide a higher confidence in the model's results.

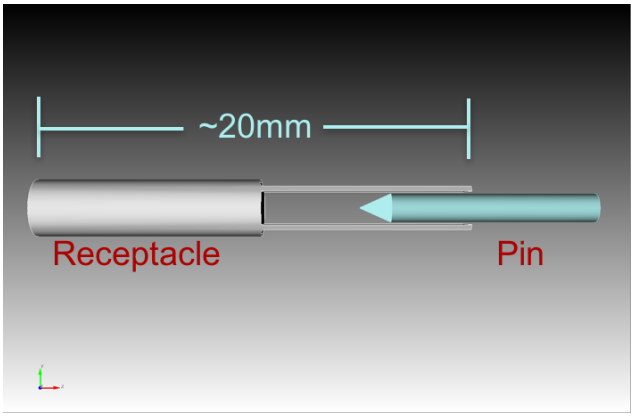

Figure 1: Diagram of Small Assembly with the Receptacle as the Test Article (left)

Several steps will be taken to provide this model validation data set:

- Dynamic ring-down testing was performed on the bifurcated receptacle in air and the results from this test were used to determine frequency and damping versus amplitude.
- The validated setup was then used to perform a dynamic ring-down test of the same system, but with varying viscosities of fluids surrounding the receptacle. The frequency and damping parameters were deduced once again for each test and the “in-fluid” results were compared to the “out-of-fluid” results to observe the effects of the fluid on the system.
- These parameters were then compared to the existing high-fidelity model to verify that the experiment and the numerical model are comparable.

The experimental setup will be described in Chapter Two, as the addition of the fluid resulted in using unconventional actuation and measurement techniques. The results of the various experiments will be examined in Chapter Three, followed by the path forward and conclusions for the study in chapter four.

Background

At Sandia National Laboratories, it is common for electro-mechanical systems to be comprised of several, separable sub-assemblies that later require assembly for operation. It is important to study these small components within larger assemblies because the success of the whole depends on the success of even the smallest of its parts. Studying small parts introduces certain complications

that larger parts do not possess. Friction may play a larger role in the system as well as effective mass. This makes smaller parts more difficult to characterize than their larger counterparts that can neglect these small-scale effects. These small parts are also more difficult to actuate and measure properly, resulting in unconventional, usually non-contact, measurement techniques. This ensures that the data acquisition system does not mass load the part in anyway and affect the characterization.

The most common solution used to maintain a continuous electrical signal for the whole system between these separated sub-assemblies is a pin and receptacle system. This study focuses on a specific assembly of a cylindrical pin that comes to a point and a two-pronged, bifurcated receptacle. This receptacle could be described as two preloaded leaf springs in a tuning fork formation, allowing for the cylindrical pin to stay in contact with the receptacle due to the elastic stiffness of the two prongs. This specific system undergoes a continuous environment of vibration and shock, so the expectation that the electrical continuity is maintained throughout the lifecycle of the system is not realistic. Due to the small contact area of the cylindrical surface with the flat surface of the receptacle, some disengagement is expected. It is the frequency that this disengagement occurs as well as its duration that could cause a concern for chatter. The system must adhere to strict temporal chatter requirements and modify the current design,

once characterized, to improve chatter dynamics to meet future chatter requirements.

There was a need for a numerical model of the system to be made to accurately predict that the system meets its chatter requirements pre-production to reduce costly redesigns. A numerical model for this system is not trivial. With the chatter behavior and the small contact patch between the pin and receptacle, it is inherent that the system is non-linear. The ROM created by Lacayo and Brake [1] consists of a mesh created in Sandia's proprietary Cubit software [2] utilizing tetrahedral elements. Only one node on both the top and bottom of the cylindrical pin were used to represent the small contact patches between the pin and receptacle. The bifurcated receptacle was modeled with a clamped-free boundary condition while the pin has a more complex boundary condition. This study only focuses on characterizing the receptacle, for test simplicity. A more complex model is desired for the future. Using the current mesh, the computational time for an explicit dynamic analysis of this system was estimated to take over a year, thus requiring a ROM to reduce computational cost. This was done using the Craig-Bampton-Hurty method. This method reduces the size of the finite element model by breaking up the degrees of freedom into boundary sets and interior sets. This is the ideal method for this model because it allows for different boundary conditions that modal decoupling does not, as well as

accounts for both mass and stiffness. process as described by Roettgen [4] , has the physical coordinates of the system represented by

$$x = \begin{Bmatrix} x_i \\ x_b \end{Bmatrix} \tag{1}$$

$$M = \begin{bmatrix} M_{ii} & M_{ib} \\ M_{bi} & M_{bb} \end{bmatrix} \tag{2}$$

$$K = \begin{bmatrix} K_{ii} & K_{ib} \\ K_{bi} & K_{bb} \end{bmatrix} \tag{3}$$

Where x is the postion vector, M is the mass matrix, and K is the stiffness matrix. Using the below transformation, the above physical coordinates can now be transformed into Craig-Bampton-Hurty Coordinates.

$$x = \begin{Bmatrix} x_i \\ x_b \end{Bmatrix} = \begin{bmatrix} \phi_{ik} & \psi_{ib} \\ 0 & I_{bb} \end{bmatrix} \begin{Bmatrix} q_k \\ x_b \end{Bmatrix} = T_{cb} \begin{Bmatrix} q_k \\ x_b \end{Bmatrix} \tag{4}$$

Where the first column contains the fixed interface modes, or the interior degree of freedom (DOF) motion when the interface boundary is fixed. The second column in (4) contains the constraint modes or, in other words, the motion of the system with a unit displacement for each DOF that is not a boundary. Lastly, q_k contains the displacements of the fixed-interface motion while x_b is carried through and contains the original boundary degrees of freedom. Using this transformation matrix, we can now get the reduced mass and stiffness matrices, detailed below.

$$M_{cb} = T_{cb}^T M T_{cb} = \begin{bmatrix} I & M_{kb} \\ M_{bk} & \widehat{M}_{bb} \end{bmatrix} \tag{5}$$

$$K_{cb} = T_{cb}^T K T_{cb} = \begin{bmatrix} \omega_k^2 & 0 \\ 0 & \widehat{K}_{bb} \end{bmatrix} \tag{6}$$

This reduced order model was not calculated by hand, rather Sandia National Laboratories' structural dynamics code, Sierra/SD [5] was implemented. The reduced mass and stiffness matrices from Sierra/SD were then put into a MATLAB code referred to as ROMULIS, developed by Dr. Matthew Brake at Sandia National Laboratories. This code takes the reduced mass and stiffness matrices for both the pin and the receptacle from the Craig-Bampton-Hurty ROM and assembles them in the diagonal global system matrices. This resulted in the following global equations of motion (EOM),

$$\begin{bmatrix} \widehat{M}_{pin} & 0 \\ 0 & \widehat{M}_{rec} \end{bmatrix} \begin{Bmatrix} \ddot{p}_{pin} \\ \ddot{p}_{rec} \end{Bmatrix} + \begin{bmatrix} \widehat{K}_{pin} & 0 \\ 0 & \widehat{K}_{rec} \end{bmatrix} \begin{Bmatrix} p_{pin} \\ p_{rec} \end{Bmatrix} = \begin{Bmatrix} \hat{f}_{pin} \\ \hat{f}_{rec} \end{Bmatrix} \tag{7}$$

where $\hat{f}$ is the transformed force vector. The method employed by the ROMULIS code goes into greater detail in [1]. The resulting system EOM are given below in (8). With this EOM, ROMULIS implements a fifth-order implicit-explicit integrator that is described by Brake in [6] that solves for the position vector $p_{f,G}$and its derivatives.

$$\widehat{M}_{ff.G}\ddot{p}_{f,G} + \widehat{K}_{ff.G}p_{f,G} = f_{f,G} - \widehat{M}_{fc.G}\ddot{u}_{c,G} - \widehat{K}_{fc.G}u_{c,G} \tag{8}$$

The creators of this model then considered the non-linear contact force between the pin and the receptacle. For the sake of simplicity, one can refer to the development of the contact force in [1] but the resulting system EOM is stated below, with the f_{NL} vector as a function of the state-variables and representation of the contact forces on the interior degrees of freedom.

$$\widehat{M}_{ff.G}\ddot{p}_{f,G} + \widehat{K}_{ff.G}p_{f,G} = f_{f,G} - \widehat{M}_{fc.G}\ddot{u}_{c,G} - \widehat{K}_{fc.G}u_{c,G} + f_{NL}(u_{e,G}, \ddot{u}_{e,G}) \quad (9)$$

The model then adds in the initial condition of the receptacle expanding and the pin coming to rest within the receptacle. The receptacle expanding is a simpler version of equation (8) that removes the mass terms and the contact force to ensure a static solution and sets the boundary conditions to fixed by assigning a null value. This results in the following initial condition.

$$\widehat{K}_{ff.G}p_{f,G} = f_{f,G} \quad (10)$$

Then, for the chatter simulations, the following initial condition is imposed

$$\widehat{M}_{ff.G}\ddot{p}_{f,G} + \hat{C}_{ff,F}\dot{p}_{f,g} + \widehat{K}_{ff.G}p_{f,G} = f_{NL}(u_{e,G}, \ddot{u}_{e,G}) \quad (11)$$

Where the added damping term simulates the elastic-plastic contact model of the pin at rest against the receptacle. Again, this initial condition ignored the initial contact force as well as imposed a fixed boundary condition as before.

Once these conditions were imposed, a chatter simulation was run. The modelers subjected the system to both shock and random vibration environments. From the results, using the upper bound of the standard deviation, it was found that the longest time interval when both prongs disengaged from the pin was well within the requirements given by the systems engineers for allowable chatter. This model is considered quite conservative, but requires

experimental validation for complete confidence as well as the further addition of the fluid effects.

The data collected in this study will be used by the creators of the above chatter model for validation and confidence, such that it can be used to aid designers in the design of future electrical contacts less prone to chatter. The data collected needs to measure properties of the system that can be directly compared to the output results from the chatter model. The properties this study aims to measure and compare are instantaneous frequency and damping versus displacement amplitude. Mode shapes of the system will also be compared. All data are extracted from measured time histories of the tests. Usually, frequency response functions (FRF) are used for these comparisons but due to the unconventional nature of the test setup, a real FRF cannot be made. These complications will be discussed in the experimental test setup section. In lieu of an FRF, a fast Fourier transform (FFT) will be calculated from the time histories of the impacts at the various measurement points. This will provide a picture of the frequency content of the various tests. The techniques used to extract these curves will be discussed in Chapter Three. Between the FFTs and the instantaneous frequency and damping curves, the modelers will have a valid data set with which to compare the model results to.

It is expected that the addition of the different fluids to the model will affect the natural frequency and damping of the electrical contact sub-assembly. The effect of a surrounding fluid should consider two parts of the fluid force; the added mass effect as well as the viscous damping effect as described in [7] [8]. In Fan *et al*'s paper [7], a piezo-driven pipette is modeled as a cantilevered beam surrounded by a viscous fluid. Sader's paper [8] also models a cantilevered beam of arbitrary cross section with a viscous fluid force surrounding it. The general fourth order beam equation is given as

$$EI\frac{\partial^4 u(x,t)}{\partial x^4} + \mu\frac{\partial^2 u(x,t)}{\partial t^2} = F(x,t) \tag{12}$$

With $F(x,t)$ separated into its viscous damping and virtual mass components, the beam equation becomes

$$F(x,t) = F_{drive} + \frac{m_{vd}du}{dt} + c_{vd}u = -M'U_o i\omega\tilde{F}e^{i\omega t} \tag{13}$$

Where M', defined below in (14), is the mass per unit length of the fluid replaced by the length of the beam. $\tilde{F}$ is also defined below in (15) where ρ_f is the density of the fluid, η is the viscosity of the fluid, $K_1$is the Bessel Function, and Re is the Reynolds number. The right side of (13) contains the real and imaginary components.

$$M' = \frac{1}{4}\pi\rho_f d_1^2 \tag{14}$$

$$\tilde{F} = 1 - \frac{4K_1\sqrt{i\beta}}{K_1\sqrt{i\beta}+\sqrt{i\beta}K_1'\sqrt{i\beta}} = Re + i\ IM \tag{15}$$

This results in the following equation of motion

$$(m + m_{vd})\frac{\partial u(x,t)}{\partial t^2} + c_{vd}\frac{\partial u(x,t)}{\partial t} + EI\frac{\partial^4 u(x,t)}{\partial x^4} = 0 \quad (16)$$

Using the approach developed by Fan *et al* [7] as an example, there are also other publications with similar fluid force approximations for numerical and analytical solutions of a cantilevered beam surrounded by a viscous fluid [9] [10] [11] [12] [13] . While many of these models are generally accepted as being valid for small cantilevered beams, they all seem to lack experimental validation due to the inherent difficulty of the unique test environments and small length scale.

From the fourth order beam equation in (12), it should be noted that it is expected that the second bending mode of a cantilevered beam should reside at a frequency six times that of the first bending mode frequency. This is a nice sanity check when evaluating the measured data to ensure that the test setup is representative of a cantilevered beam system. This test article resembles a tuning fork formation, as mentioned before. As such, it is expected from the system that there will be out-of-phase bending modes and corresponding in-phase bending modes. Analytically, these two out-of-phase and in-phase modes should be at the same frequencies, but in the physical system there are factors, such as damping and boundary conditions, that do not allow these in-phase and out-of-phase modes to lie at the same frequency. In the physical system, the in-phase bending mode, pictured in Figure 2 (left), is expected to be at a slightly lower frequency than its out-of-phase counterpart, pictured in Figure 2 (right),

because the tines that are moving in-phase will deform the base more than the out-of-phase mode tines moving out-of-phase.

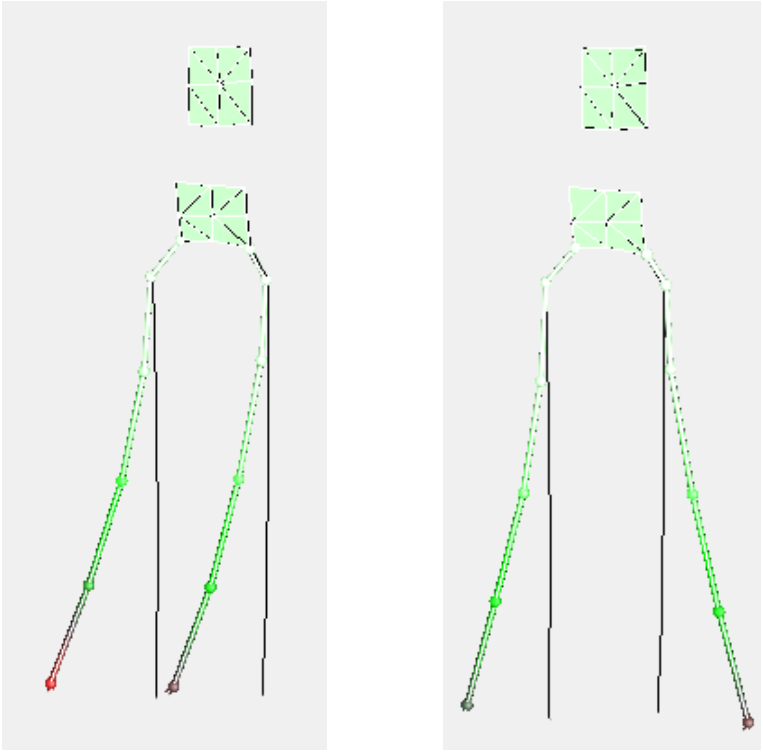

Figure 2: In-phase and Out-of-phase First Bending Mode Shapes of a Tuning Fork

Chapter Two: Experimental Setup

This experiment posed inherent challenges due to the small scale of the part being tested and the fluid within the test cell. Dynamic ring-down testing was performed to characterize the properties of the part. A fixture design was created to accommodate both needs and is pictured below without the part in the fixture.

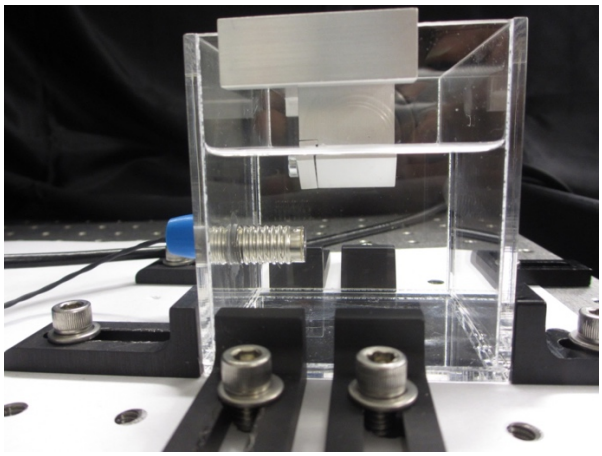

Figure 3: Test Setup with Oil

The addition of the fluid makes for an unconventional test setup, as the actuator method and the measurement method both need to tolerate this liquid environment. For the issue of actuation, an encapsulated piezo-electric actuator was acquired. The Encapsulated PICMA® Stack Piezo Actuators are manufactured by the German company Physik Instrumente (PI) and are pictured in both Figures 3 and 4. The operating specifications are listed below in Table 1. This actuator can be submerged in a liquid environment as well as high humidity environments where other piezo-electric equipment may not perform well. Another benefit to this encapsulated actuator is that it already pre-loaded, making

the test setup easier and safer. The version of the actuator chosen was the P-885.55.

Table 1: Specifications for the PICMA Stack Actuators [14]

Part Number	Dimensions OD x L [mm]	Nominal displacement [μm] (0-100V)	Max. displacement [μm] (0-120V)	Blocking Force [N] (0-120V)	Stiffness [N/μm]	Electrical Capacitance [μF]$\pm$20%	Resonant Frequency [kHz] $\pm$20%
P-885.55	11.2 x 22.5	14$\pm$10%	17$\pm$10%	850	50	1.5	60
P-885.95	11.2 x. 40.5	30$\pm$10%	36$\pm$10%	900	25	3.1	35
P-888.55	18.6 x 22.5	14$\pm$10%	17$\pm$10%	3400	200	6.0	60

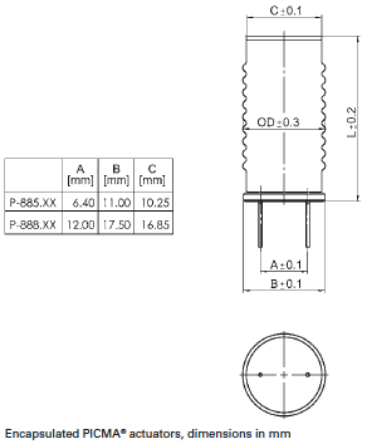

Figure 4: Technical Drawing for the PICMA Stack Actuator [14]

A voltage was applied to the actuator with a custom signal to simulate an impulse while also reducing the effects of the actuator pulling away from the part. This signal is shown in Figure 5. Unfortunately, the actuator was not able to physically hit the receptacle due to tolerances between the test setup and the actuator displacement. The actuator only displaces approximately 14 micrometers, making it difficult to get the part close enough to the actuator to have it touch when actuated, but not touching when at rest. Fortunately, the PICMA could actuate the air and fluid surrounding the receptacle enough to get a measurable response. This part of the setup needs to be better developed for future testing.

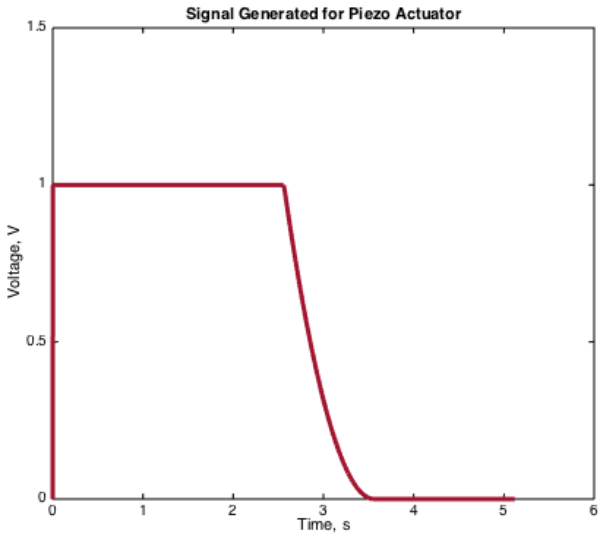

Figure 5: Actuator Signal

A Laser Doppler Vibrometer (LDV) was used to measure the response of the dynamic ring-down tests. The LDV used is a Polytec PSV-400 LDV and is a one-dimensional measurement system. An LDV uses an optical transducer to determine vibration velocity and displacement at specified points on a subject of interest. A neon laser beam is first split into two parts, a measurement beam and a reference beam. The measurement beam then gets split again and is focused onto the subject of interest, in this case, the bifurcated receptacle, which then reflects the beam back to the second beam splitter. A final splitter then deflects the measurement beam back into the reference beam and deflects it onto the detector. A diagram for this process is shown in Figure 6 and a picture of the system used is shown in Figure 7. A more detailed explanation of the physics utilized in the LDV can be found in [15] . A close-up module was used in this study; it acts as an extra focusing lens. The receptacle is very small and this

ensured the laser would be able to focus on the part successfully. Another factor to consider for the LDV was measuring through plexiglass as well as the additional fluid. Some test setup fine-tuning was required to ensure the beam was focusing correctly as well as not interfering with itself. Some calculations for finding the exact α angle that the laser is pointed at with respect to the normal of the part surface are found in [16] [17].

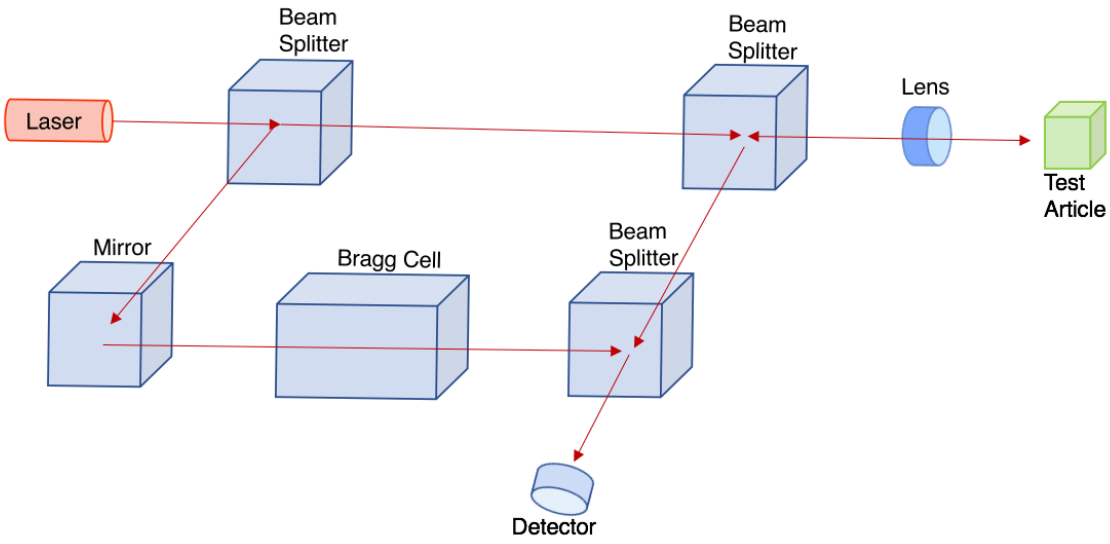

Figure 6: How LDV Takes Measurements

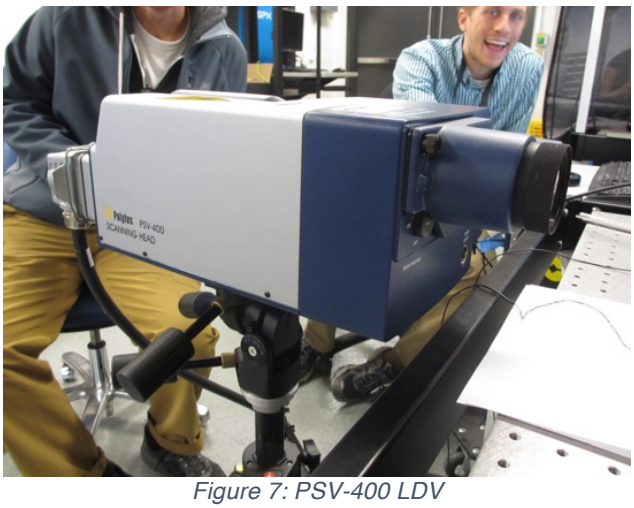

Figure 7: PSV-400 LDV

The LDV was controlled by Polytec's proprietary system. Within the system's software, a two-dimensional laser alignment was performed on the bifurcated receptacle and several parameters were set for the measurement properties, listed in the Appendix for both a time history measurement and a fast-Fourier transform (FFT) measurement. This system was also able to produce the wave form, from Figure 5, for the piezo-electric actuator. This wave-form was put through a high-voltage amplifier to control the signal going to the piezo-electric actuator. The high-voltage amplifier is pictured below in Figure 8. The measurement points are set by the user within the software and the laser focus is double checked at each point to ensure the quality and success of the measurement.

Figure 8: High Voltage Amplifier

A dynamic ring-down test was performed in air as well as in a representative fluid. It was determined that several levels of fluid viscosity would be tested to see the effects of the different viscosities, which also simulates changing temperature. The fluid in the actual system has a viscosity level of about 15 cst. A commercial off-the-shelf silicon oil was chosen to be a close approximation to

the actual fluid that could not be included here for sensitivity purposes. The oils chosen are XIAMETER® PMX-200 Silicone Fluid in both 10cst and 20cst viscosities with relative densities of 0.934 and 0.95 respectively. These silicone oils are produced by Dow Corning and their product information can be found in [18] and [19]. Currently, this experiment only has data for the dynamic ring-down in air, the 10cst fluid, and the 20cst fluid. The measured response data will provide insights as to the effects of fluid in the system.

Once the bifurcated receptacle is placed in the test fixture, the appropriate fluid is added, the test can begin. The wave form is supplied to the amplifier and the actuator. The LDV then scans each point that was determined by the user in the setup and either produces a time history for each point on the geometry or an FFT. The time history data can then be post-processed using a short-time Fourier-transform (STFT) method that will be described in Chapter Three. The FRF cannot be calculated from this test setup due to not being able to directly measure the input force. Therefore, only operating deflection shapes (ODS) can be obtained from the data, providing measured representation of physical mode shapes.

An issue with this test setup is that only one tine of the receptacle can be measured at a time. To verify the different in-phase and out-of-phase modes, a 1D measurement was taken from both tines at an angle and then the 3D

coordinates were transformed in the post-processing. This process is described in the results section. A 3D LDV was also used towards the end of this study to verify mode shapes of both tines with a third method. The data collection process is utilizing a 3D LDV is similar as described above, with some minor changes in the LDV alignment process.

(This space intentionally left blank)

Chapter Three: Results

Data and Processing

Time history and fast Fourier transform (FFT) data was measured during impact testing with a frequency bandwidth of 20 kHz. This large bandwidth ensured that the second bending modes were measured as well as any other modes that could potentially be excited within this range with this test setup. Figures 9 through 11 show the entire FFT for each setup in air, 10cst oil, and 20cst oil. These were taken directly from the Polytec data acquisition system. In air, the first bending modes are very excited while the higher modes are not as excited, therefore, this study will only focus on the first bending modes. Also, with increasing viscosity of fluid, damping increases and there is a softening in the frequencies of the excited modes, indicating a non-linear response. It is to be noted that the higher modes seem to be slightly more excited in the oil environments. Figures 12 and 13 show the first and second in-phase bending mode shapes, at 1030 Hz and 6525 Hz, respectively.

(This space intentionally left blank)

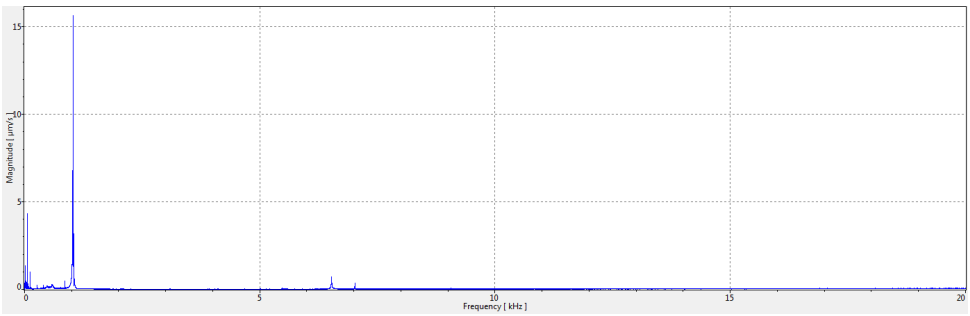

Figure 9: Frequency Content in Air (FFT)

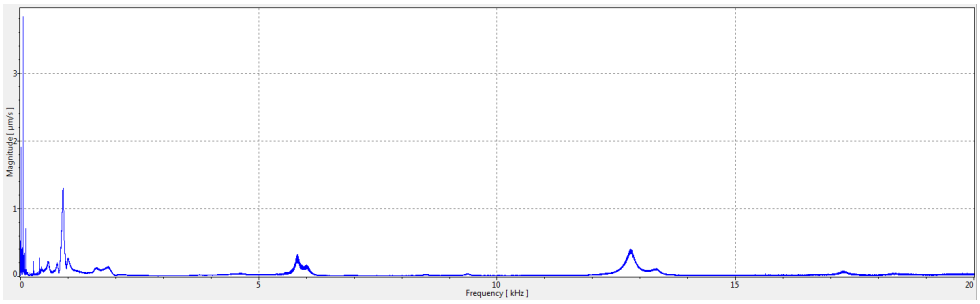

Figure 10: Frequency Content in 10cst Oil (FFT)

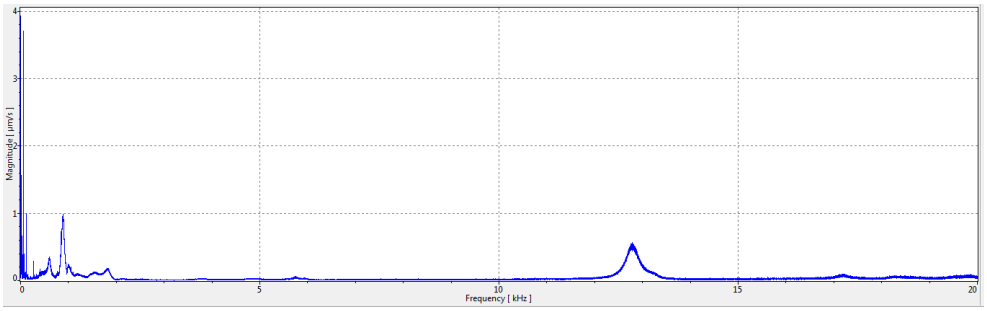

Figure 11: Frequency Content in 20cst Oil (FFT)

Figure 12: First Bending Mode from 1D LDV

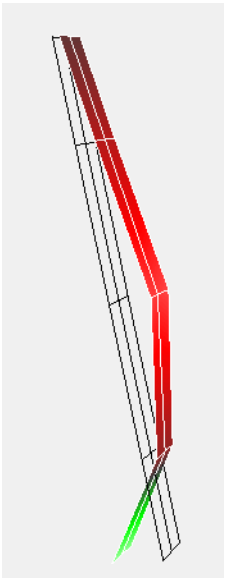

Figure 13: Second Bending Mode from 1D LDV

The processing of the 1D LDV data was performed using the Short Time Fourier Transform GUI (STFT) developed by Robert Kuether at Sandia National Laboratories. This GUI uses short windowing of the time history signal and the LDV measured velocity to extract the amplitude of the signal as well as the instantaneous frequencies and damping ratios of a mode of interest. To use the STFT GUI, a time history of an impact test must be measured. From that time history, the abscissa and ordinate represent the time and velocity respectively. The user must then choose a cut-off frequency for the extraction that will include the modes of interest and the data is then windowed. This data was calculated using a Hanning window between 0.1 and 1 second. The Hanning window is used because the signal needs to begin and end at zero with a slope of zero in order to maintain periodicity. The Hanning window is also advantageous due to its accelerated roll-off rate of 18 dB per octave, decreasing the side-lobe of the signal. Using these settings, the spectrogram of the signal and the STFT can be calculated. An example of the GUI can be found in Figure 14. A tight frequency bandwidth around the frequency of the mode of interest must be set for the harmonics to be extracted for that mode.

(This space intentionally left blank)

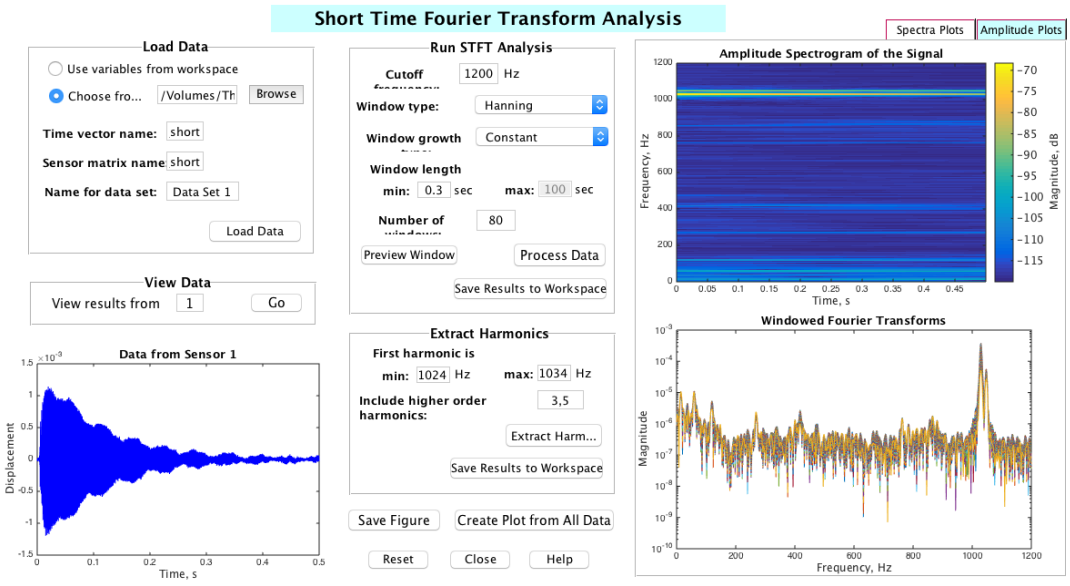

Figure 14: Example of STFT GUI Window

Figures 15, 17, and 19 show the FFT zoomed in on the first two complimentary bending modes of the system in air, 10cst oil and 20cst oil from the Polytec system. As described earlier, this receptacle can be compared to a tuning fork, and it is expected that it will have in-phase bending modes and corresponding out-of-phase bending modes at slightly higher frequencies than their counterparts. These complimentary modes will be investigated further on in this chapter using 3D measurements. Frequency softening and increased damping is observed between the FFTs as well as a separation of the complimentary modes' frequencies. As discussed by Green [10] , this is likely due to the effective mass changes from the addition of the fluid rather than the viscous damping effects. Figures 16, 18, and 20 show the results of using the STFT GUI on the first bending modes in air, 10cst oil, and 20cst oil respectively. Exact values for the frequencies and averaged values for the damping ratios are in Table 2.

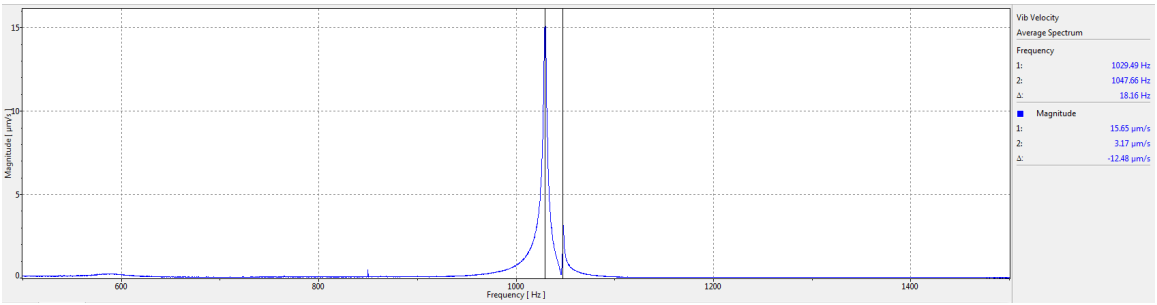

Figure 15: FFT - First Bending Modes in Air

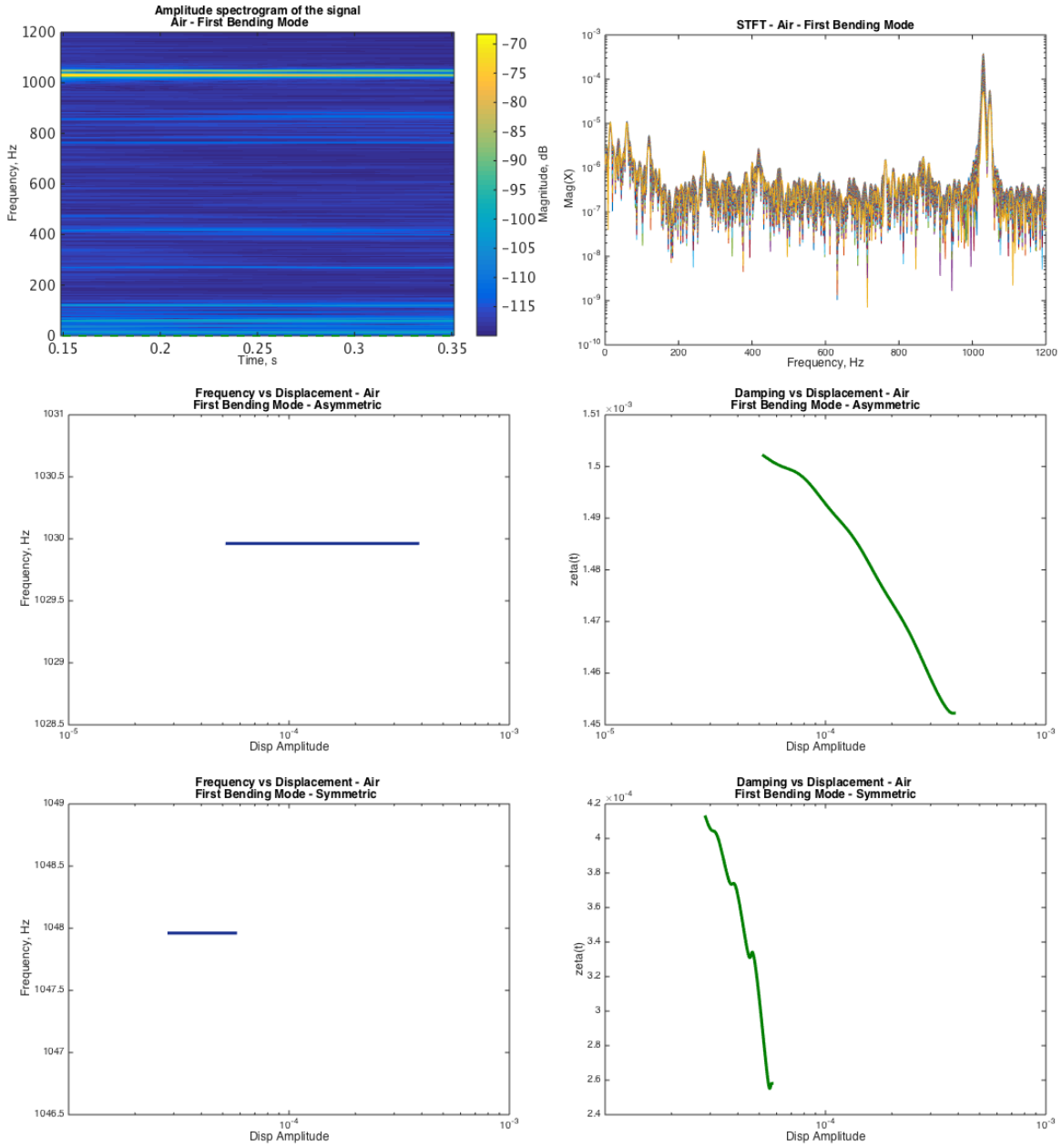

Figure 16: STFT of First Out-of-phase and In-phase Bending Modes in Air

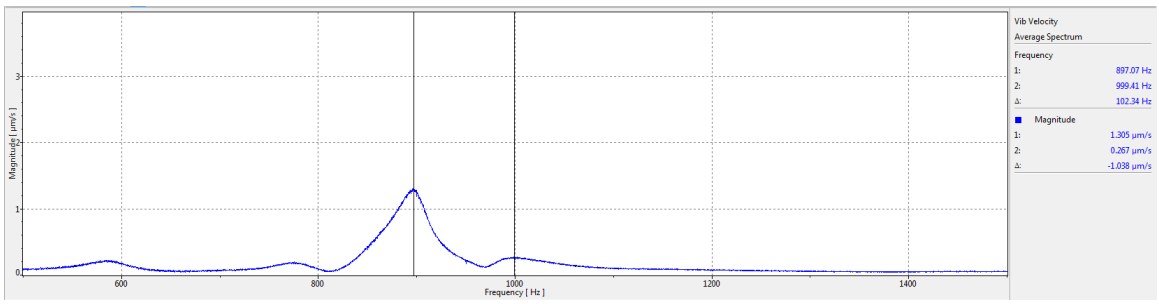

Figure 17: FFT - First Bending Modes in 10cst Oil

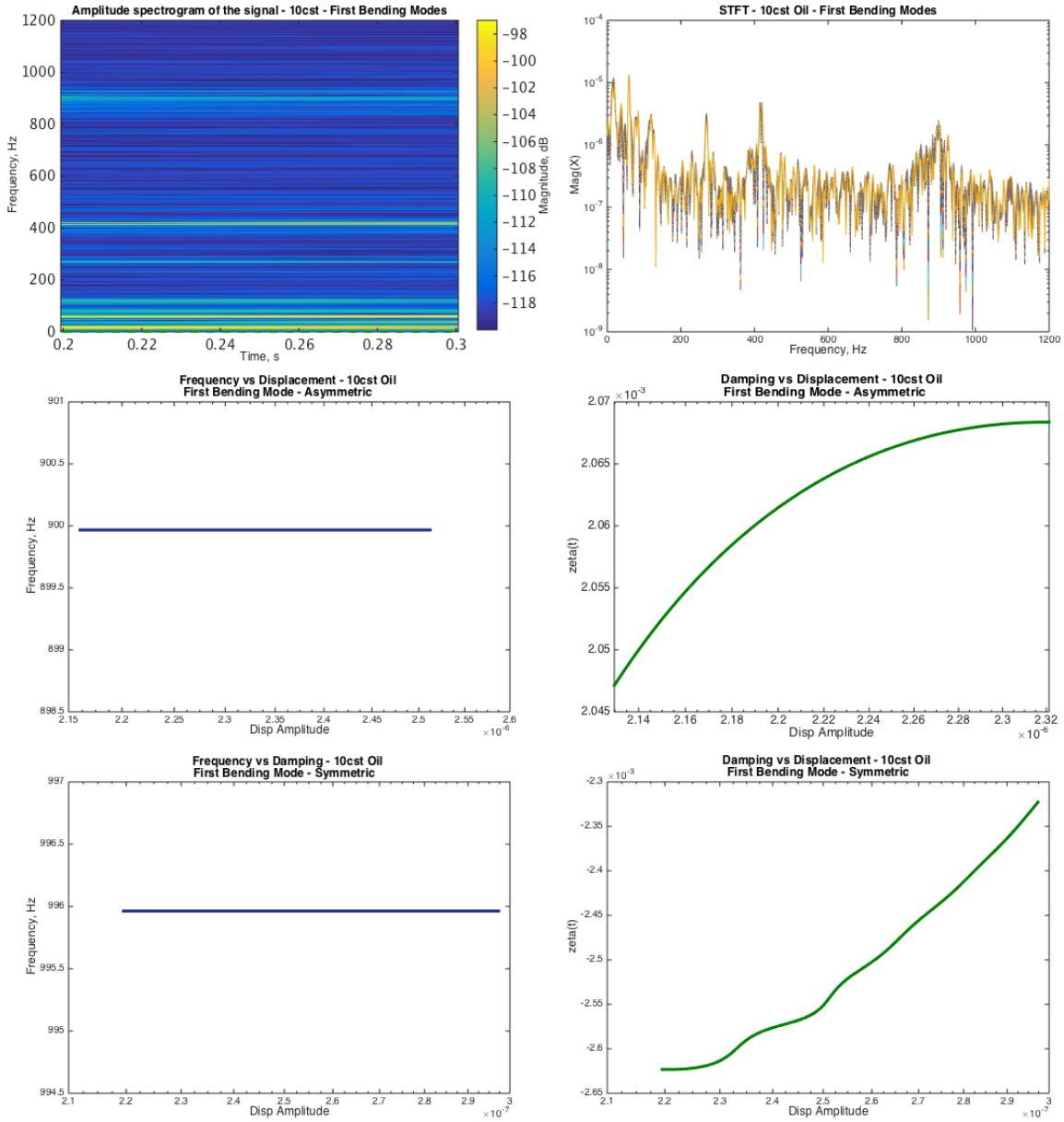

Figure 18: STFT of First Out-of-phase and In-phase Bending Modes in 10cst Oil

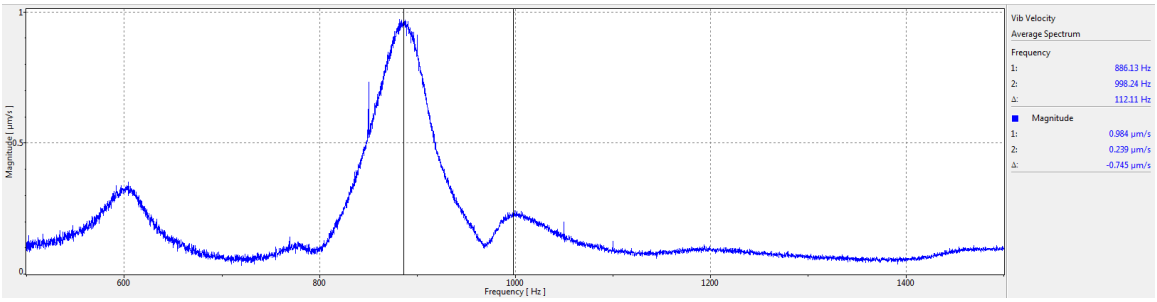

Figure 19: FFT - First Bending Modes in 20cst Oil

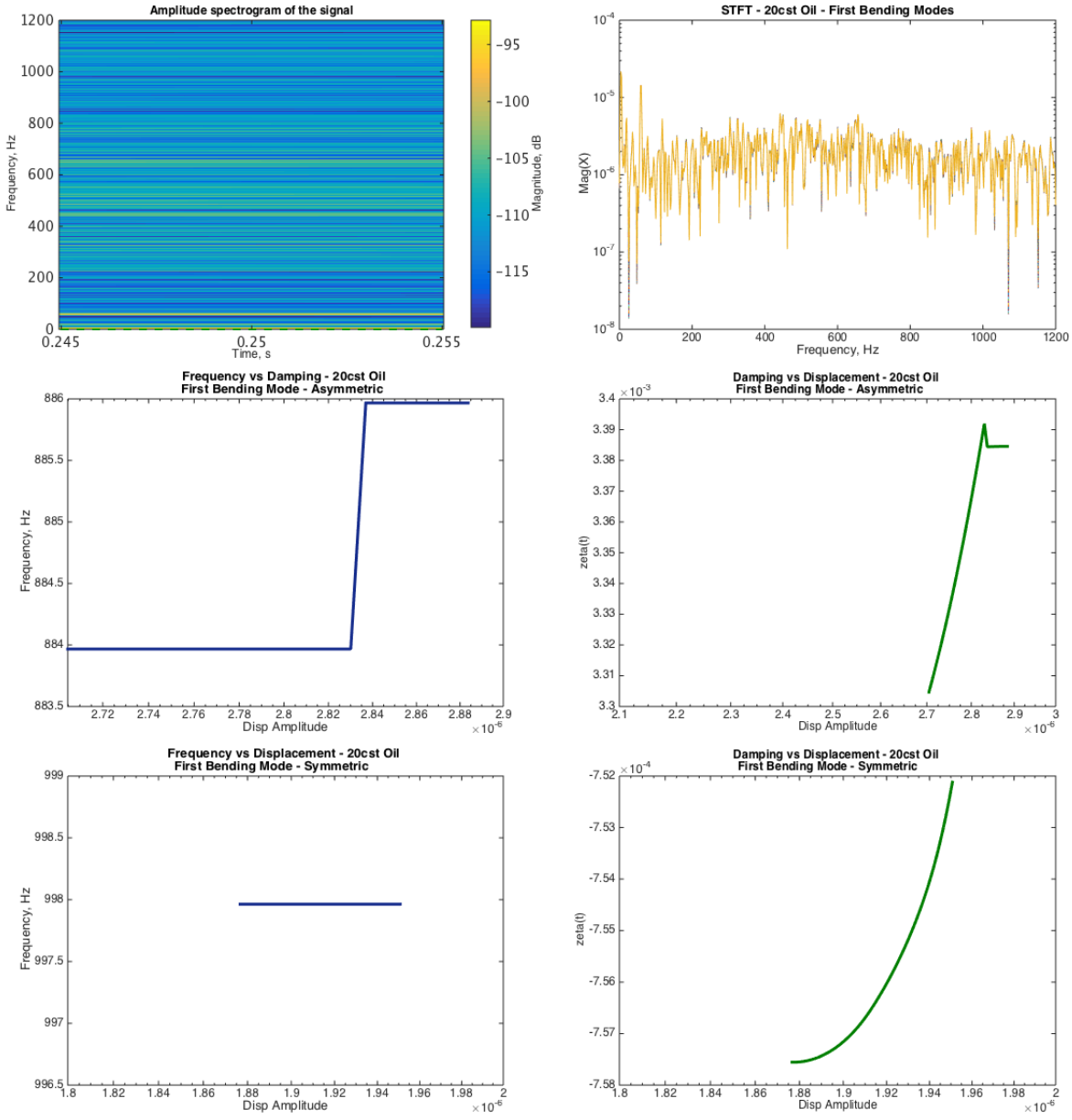

Figure 20: STFT of First Out-of-phase and In-phase Bending Modes in 20cst Oil

Table 2: Instantaneous Frequency and Damping for First Bending Modes

	AIR (IN-PHASE)	AIR (OUT-OF-PHASE)	10CST (IN-PHASE)	10CST (OUT-OF-PHASE)	20CST (IN-PHASE)	20CST (OUT-OF-PHASE)
FREQUENCY	1030.00 Hz	1048.00 Hz	899.97 Hz	995.96 Hz	884.17 Hz	997.96 Hz
DAMPING (ζ)	0.0015	0.0003477	0.0021	0.0019	0.0034	0.0007557

With increasing oil viscosity, there is an increase in the measurement noise, which is most obvious in the spectrogram and STFT of the 20cst data. The code is also having difficulty finding the first in-phase bending mode frequency peak in the 20cst oil. This is likely due to the displacements being damped by the oil as well as the oil movement continuing past the actuation signal, causing more actuation in various directions. There are also more fixture modes measured in oil than in air. Again, this is likely due to fluid movement during the measurements.

As mentioned before, there are two tines to the receptacle, but with the 1D LDV, it is usually only measuring normal to one tine. Thus, a 3D measurement is needed to confirm the mode shapes are either in-phase or out-of-phase. A first attempt at this was to move the LDV at an angle to the test fixture and align the measurement points along the outside surface of the front tine and along the inside surface of the back tine. Then, using the measured data, the 2D coordinates were transformed in MATLAB to 3D coordinates and then a mode shape correlation algorithm was implemented. This method was chosen over polynomial fitting because the latter is not ideal for the receptacle's in-phase and out-of-phase, closely spaced modes. The algorithm used,

Synthesize Modes and Correlate (SMAC), was developed at Sandia National Laboratories by Randy Mayes [20] . It is ideal for extracting weakly excited modes as well as the closely spaced modes because it is not limited to the FRF resolution. More details of this modal extraction algorithm can be found in Mayes' papers. The function is also commercially available in the IMAT toolbox of MATLAB.

There were three separate lines of points selected for this measurement, two lines on the front tine and one line on the back tine. This was because it was difficult to get more lines on the back from the measurement angle. Then, in MATLAB, these lines were given their 3D coordinates and SMAC extracted the two first bending mode shapes in air. The results of this are shown in Figures 21 and 22. This measurement confirmed that, of the two first bending modes of the system, the one with the lower frequency is the in-phase mode that deforms the base more, and the higher frequency mode is the out-of-phase mode.

(This Space Intentionally Left Blank)

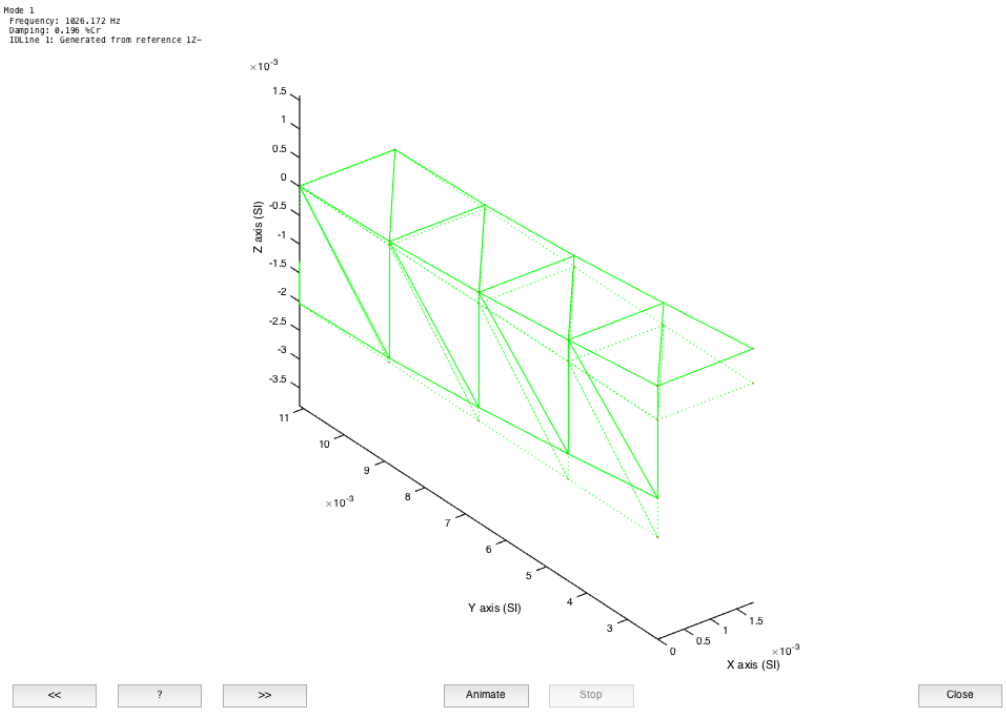

Figure 21: SMAC Extraction - First Bending Mode, In-phase

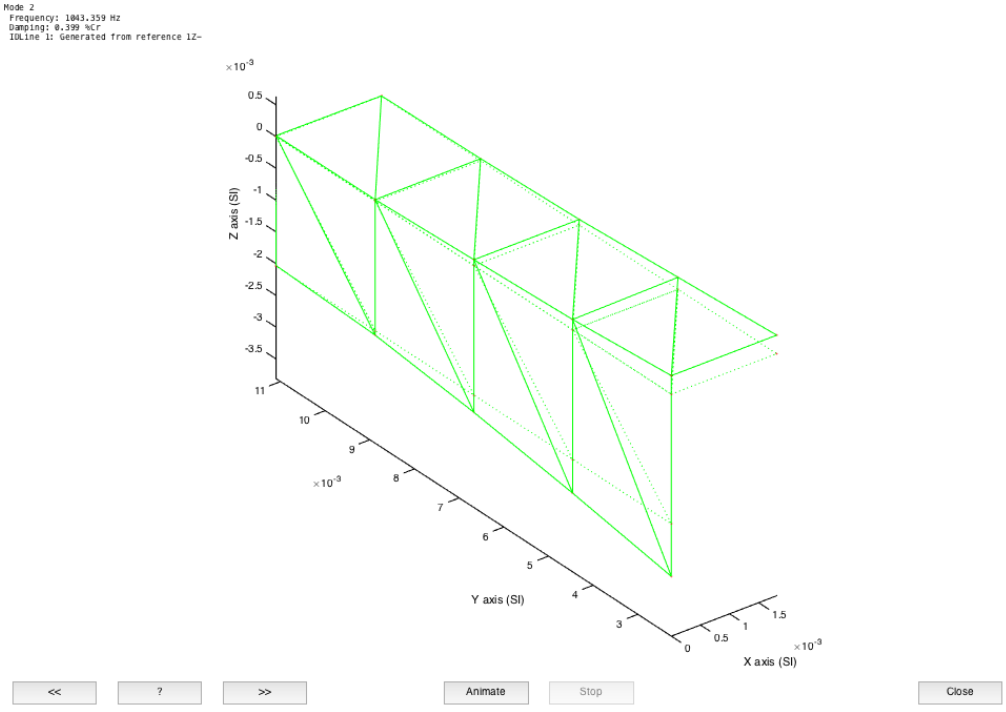

Figure 22: SMAC Extraction - First Bending Mode, Out-of-Phase

A third method, the 3D LDV, was used to confirm this data. The measurements were taken using the Polytec PSV-500 LDV, which utilizes three laser heads as opposed to the previous data being taken by only one laser head. This laser is more powerful and more precise than the older system, so measurements could be taken along the thin edges of each tine. The frequency content is shown in Figures 23 and 24 and the mode shapes are shown in Figure 25. This 3D LDV data agrees with the rest of the measured data in this study as well as the assumptions of the in-phase and out-of-phase modes. Both 3D confirmation methods were only performed on the test article in an air environment.

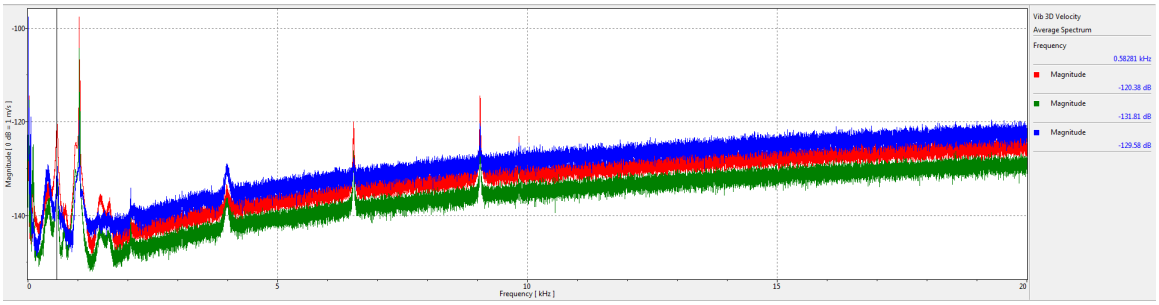

Figure 23: FFT from 3D LDV Measurement in Air

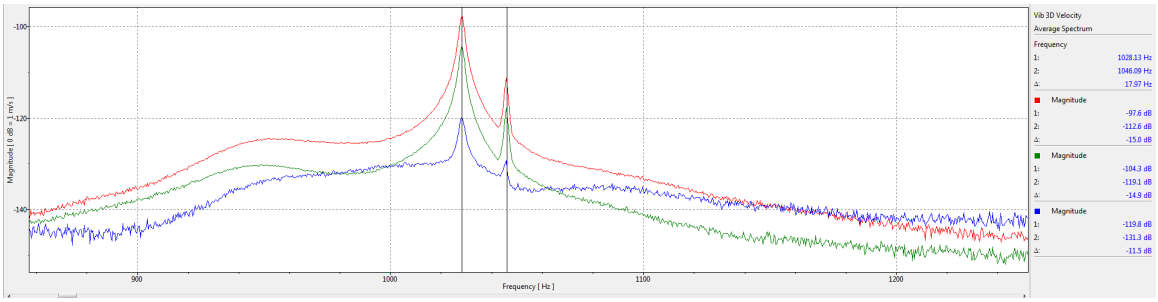

Figure 24: FFT - First Bending Modes in Air from 3D LDV

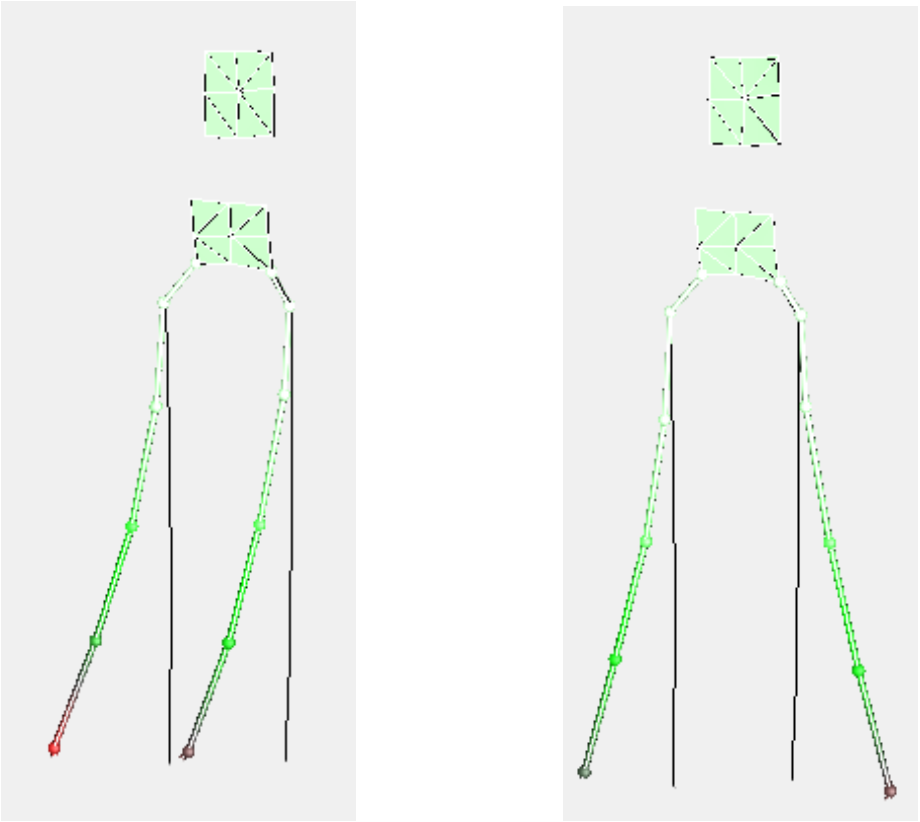

Figure 25: Out-of-Phase First Bending Mode (left) and In-Phase First Bending Mode (Right) from 3D LDV

Model Comparison

A high-fidelity model was created by Dr. Jill Blecke of the bifurcated receptacle in 2013 [21]. The frequencies she estimated in her model follow the same trend as the frequencies measured in this study with minimal error. A table of values comparing the frequencies of the first bending modes from the model and the measured data can be found in Table 3. There is a difference of approximately 20 Hz between the model and the measured data with an error of under 2%. This error could be due to many things, but most likely due to the fixturing of the test article in this study. The model is much more rigidly fixed than can be achieved in the physical test setup as well as the fixed nodeset in the model being in a

different location than the clamping location in the test setup. The model's material properties, such as modulus of elasticity, also have an inherent error, usually of +/- 5%. Completing a statistical study on varying the material properties within the error bound could yield insights as to how much that error affects the output from the model. Future work should also include changing the fixed boundary condition location in the model to better reflect the test as well as improving the test receptacle fixed boundary condition, potentially utilizing epoxy or another adhesive. The model could also be used to investigate the effect of rigidity in the base of the receptacle on dynamic response.

Table 3: First Bending Mode Frequency Comparison between Model and Data

	AIR – FIRST BENDING MODE (IN-PHASE)	AIR – FIRST BENDING MODE (OUT-OF-PHASE)
HIGH FIDELITY MODEL FREQUENCY	1046.20 Hz	1053.70 Hz
MEASURED FREQUENCY DATA	1030.00 Hz	1048.00 Hz
% ERROR	1.74 %	0.54 %

Additional future work is to improve the actuation technique. A measureable input force would be ideal to extract the FRFs and have a better comparison between model and experiment. This could be done by improving the tolerances in the test setup to ensure the piezo-actuator can hit the part while not touching the part at rest. A different excitation method could also be investigated. One method of interest would be the use of a 6 degree of freedom shaker. This type of testing would better simulate the vibration and shock environments that the real system sees, rather than separating the testing into different axes. Acoustic or ultrasound excitation could also be investigated.

Chapter Four: Conclusion

The current state-of-the-art method for predicting chatter in a small electrical system is a numerical method that employs an implicit-explicit approach. However, there is no experimental validation that can give this method complete confidence. This research provided a high-fidelity model of the system in air with a validation data set as well as provided new information for the numerical modelers when it comes to the non-linear fluid effects of the system. This data showed how the addition of fluid induces a frequency softening effect as well as separates the complimentary in-phase and out-of-phase bending modes of the system.

While there was only small error between the measured data and the model, the test setup could be improved to better represent the real system as well as updating the model's original assumptions of the fixed boundary and material properties. This kind of experimental validation, paired with modeling efforts, is crucial to the design process of small components within larger assemblies, and its accuracy will better improve the confidence of the design process. The actuation and measurement in this study utilized unconventional techniques that have previously not been used on this system due to the small length scale and the fluid environment. The development of these techniques for this purpose will help other small component testing that need experimental validation in unique

environments. This study hopes to encourage pre-manufacturing validation, reducing costly and inefficient redesigns as well as push forward experimental techniques on small scales and in unique environments.

Appendix

Polytec PSV-400 Time History Measurement Settings

PSV **File Information** Date: Monday, March 06, 2017 Time: 1:44:19 PM
Polytec Scanning Vibrometer

Name:	D:\kmjohn\Contact\SEC_kmjohn_122016_air_time_0pt5V.svd
User:	Modal
Created:	Date: 12/20/2016 Time: 3:26:29 PM
File version:	9.00
Application version:	9.0.4.0

Comment

Scan Points

Total:	15	
Not Measured:	0	0.0 %
Valid:	14	93.3 %
Overrange:	1	6.7 %
Invalidated:	0	0.0 %
Disabled:	0	0.0 %
Not Reachable:	0	0.0 %
Hidden:	0	0.0 %
VT Failed:	0	0.0 %

Hardware

Scanning Head :	PSV-I-400 MR (OFV-505)
Firmware version:	1.20
Junction Box:	PSV-E-401-M4
Firmware Version:	2.1
Acquisition Board:	National Instruments PCI-6110
Channels Count:	4
Highest Sample Frequency:	2.56 MHz
Function Generator	
Channels Count:	1

General

Acquisition Mode:	Time
Averaging:	Off
Remeasure Automatically:	Active
AutoRange:	Not active
PCA (MIMO):	Not active
Cosine correction X:	Active
Cosine correction Y:	Active

Sampling

Sample length:	65536

Range:	VD-09 5 mm/s/V
Low pass filter:	Off
High pass filter:	Off

Displacement output

Range:	DD-900 50 nm/V

Function Generator 1

Type:	NI 611x
Signal:	User Defined
Frequency:	195.3125 mHz
Amplitude:	500 mV
Offset:	100 mV
Waveform file:	C:\Users\M...\Step_Kelsey.txt
Multiple Channels:	Off

References

[1] R. M. Lacayo, "Title Omitted, SAND2015-1647 (OUO)," Sandia National Laboratories, Albuquerque, NM, 2015.

[2] Sandia National Laboratories, "Cubit 14.1," 2014. [Online]. Available: https://cubit.sandia.gov/public/documentation.html.

[3] R. R. Craig and M. Bampton, "Coupling of Substructures for Dynamic Analysis," *AIAA Journal,* vol. 6, pp. 1313-1319, 1968.

[4] D. e. A. Roettgen, "A Comparison of Reduced Order Modeling Techniques Used in Dynamic Substructuring," *Dynamics of Coupled Structures,* vol. 4, 2016.

[5] H. C. Edwards, "Sierra Framework Version 3: cOre Services Theory and Design, SAND2002-3616," Sandia National Laboratories, Albuquerque, NM.

[6] M. R. W. Brake, "IMEX-a: An Adaptive, Fifth Order Implicit-Explicit Integration Scheme, SAND2013-4299," Sandia National Laboratories, Albuquerque, NM, 2013.

[7] M. e. A. Fan, "Vibration Study of the Piezodriven Pipettes Immersed in Viscous Fluids," *Journal of Applied Physics,* vol. 100, no. 074701, 2006.

[8] J. E. Sader, "Frequency Response of Cantilever Beams Immersed in Viscous Fluids with Applications to the Atomic Force Microscope," *Hournal of Applied Physics,* vol. 84, no. 1, 1998.

[9] C. P. S. J. E. Green, "Frequency Response of Cantilever Beams Immersed in Viscous Fluids Near a Solid Surface with application to the Atomic Force Microscope," *Journal of Applied Physics,* vol. 98, no. 114913, 2005.

[10] C. P. S. J. E. Green, "Small Amplitude Oscillations of a Thin Beam Immersed in a Viscous Fluid Near a Solid Surface," *Physics of Fluids,* vol. 17, no. 073102, 2005.

[11] S. R. A. Basak, "Hydrodynamic Loading of Microcantilevers Vibration in Viscous FLuids," *Journal of Applied Physics,* vol. 99, no. 114906, 2006.

[12] E. O. Tuck, "Calculation of Unsteady Flows fue to Small Motions of Cylinders in a Viscous Fluid," *Journal of Engineering Mathematics,* vol. 3, no. 1, 1968.

[13] C. A. S. J. E. Van Eysden, "Small Amplitude Oscillations of a Flexible Thin Blade in a Viscous Fluid: Exact Analytical Solution," *Physics of Fluids,* vol. 18, no. 123102, 2006.

[14] *Encapsulated PICMA(R) Stack Piezo Actuators,* Lederhose: PI Ceramic, 2016, p. 9.

[15] P. Inc., *Polytec PSV 400 1D Scaning Laser Vibrometer,* Irvine, CA: Polytec Inc., 2009.

[16] P. Inc., *LDV Measurments through Windows,* Irvine, CA: Polytec Inc., 2005.

[17] P. Inc., *3D Vibration Measurements of Submersed Objects,* Irvine, Ca: Polytec Inc..

[18] D. Corning, *XIAMETER(R) PMX-200 Silicone Fluid 10 CS Safety Data Sheet,* 2017.

[19] D. Corning, *XIAMETER(R) PMX-200 Silicone Fluid 20 CS Safety Data Sheet,* 2017.

[20] R. L. J. D. D. Mayes, "A Modal Parameter Extraction Algorithm Using Best-Fit Reciprocal Vectors," Sandia National Laboratories, Albuquerque, NM, 1998.

[21] J. C. W. M. C. Blecke, "Title Omitted, SAND2015-2032," Sandia National Laboratories, Albuqerque, NM, 2015.

[22] N. R. E. K. B. J. Weiss, "Modeling of a Clamped-Clamped Beam Vibrating in a Fluid for Viscosity and Density Sensing Regarding COmpressibility," *Sensors and Actuators,* vol. A 143, pp. 293-301, 2007.

[23] V. Y. B. M. M. Blouin, "Redesign of Submerged Structures by Large Admissible Perturbations," *Journal of Off-Shore Mechanics and Arctic Engineering,* vol. 123, p. 103, 2001.

[24] D. J. Inman, Engineering Vibration, Prentice-Hall inc., 1994, pp. 318-322.

[25] R. J. B. M. R. W. Kuether, "Instantaneous Frequency and Damping from Transient Ring-Down Data," in *International Modal Analysis Conference XXXIV*, Orlando, FL, 2015.

[26] "Hanning Raised Cosine," [Online]. Available: https://ccrma.stanford.edu/~jos/sasp/Hann_Hanning_Raised_Cosine.html.